and structural testing–aerodynamic research wing 1. This model consists of 10 structural modes, which are represented by 20 states. The aerodynamics (for Mach number $M = 0.9$) are represented using Roger's rational approximation[7] involving two lag terms. This leads to an additional 20 states, which will be referred to as aerodynamic states. The aileron is activated by a third-order actuator, which contributes another three states. Finally, the system is assumed to be subjected to atmospheric turbulence, which is modeled by the Dryden gust spectrum. This yields two additional states. We therefore end up with a plant having a total of 45 states. Clearly, any LQG design results in a controller of order 45. Attempts will be made in the following to apply our procedure to this example in order to come up with a controller having a lower order, with negligible effect on its performance. The full-state feedback LQG design was obtained in this example using the fictitious noise adjustment procedure[5] for robustness improvement. The flutter dynamic pressure for the closed-loop case at $M = 0.9$ is given by $Q_F = 191$ psf. This compares with $Q_F = 96$ psf obtained for the open-loop case. The LQG design point for this example is at a dynamic pressure $Q_D = 156.9$ psf. The minimum singular value of the return difference in this single-input–single-output example is $\sigma_{\min} = 0.886$. The control surface activity at the design point, due to a 1-ft/s gust velocity, is given by $\delta = 4.22$ deg and $\dot{\delta} = 183$ deg/s, with performance index $J = 5484$ (obtained with $R = 10^{-6}$ and $Q = 0$). The LQG design yields the full-state matrices $\boldsymbol{F}$ and $\boldsymbol{L}$, and, therefore, the first step of the design procedure has been achieved (note that $\boldsymbol{F}$ is not strictly required for this first step).

Application of Proposed Method to Plant-Controller System

Steps 2–6 of the proposed procedure are now followed, leading to the transformed set of equations in terms of z states. The results obtained using steps 2–6 of the proposed procedure are presented in Table 1 and reveal the important z states in the plant-regulator feedback system. As can be seen from Table 1, the important z states are the following: 1–7 and 43–45. This yields a total of 10 important states. Finally, we proceed with steps 7–10 of our procedure, using the just determined 10 important z states. The results are summarized in Table 2. As can be seen, the value of J for the 10th-order controller ($J = 5505$ with a total of 55 states for the plant-controller system) is essentially the same as the value obtained using the full-order controller ($J = 5484$, with a total of 90 states for the plant-controller system). The control surface activities and the flutter dynamic pressure are identical for both full- and reduced-order controller systems, with only small differences observed in the values of $\sigma_{\min}$. For the full-order controller, $\sigma_{\min} = 0.886$, compared with $\sigma_{\min} = 0.835$ for the 10th-order controller. The root-locus and Nyquist plots for the reduced-order controller (not shown) are essentially identical to the root-locus and Nyquist plots for the full-order controller.

Table 1 Numerical values of the component cost ψ_i in the z space for the closed-loop plant-regulator system, $J = 1070.13$

ith z coordinate	ψ_i	ith z coordinate	ψ_i	ith z coordinate	ψ_i
1	−247.53	16	0.13	31[a]	0.29
2[a]	31.01	17[a]	0.00	32	3.61
3[a]	−504.05	18[a]	0.00	33[a]	−0.97
4	−538.58	19[a]	5.57	34[a]	3.47
5[a]	2404.94	20[a]	−1.13	35[a]	0.50
6[a]	−565.16	21	0.12	36[a]	−1.28
7	803.66	22	−0.12	37[a]	0.00
8[a]	5.26	23[a]	−0.54	38[a]	0.00
9[a]	−1.25	24[a]	−0.01	39[a]	0.38
10	0.16	25	0.00	40[a]	0.90
11[a]	0.00	26	0.00	41[a]	−0.51
12[a]	0.00	27	−0.05	42[a]	3.41
13	−0.01	28[a]	0.64	43[a]	4420.55
14[a]	−0.25	29[a]	2.35	44[a]	−73.88
15[a]	−0.67	30[a]	1.89	45	−4682.73

[a]Denotes pairs of conjugate eigenvalues in reconstruction error matrix.

Table 2 Summary of plant-controller results

No. of observer feedback $\hat{z}$ states	J	Q_F, psf	$\sigma_{\min}$	δ, deg	$\dot{\delta}$, deg/s	Remarks
45	5484	191	0.886	4.22	183.0	Full-state controller
10	5505	191	0.835	4.23	183.5	Truncated controller
0	1071.7	——	——	1.84	169.2	Regulator with 10 feedback z states

Conclusions

The proposed method enables the order reduction of LQG designed controllers, with negligible effects on the closed-loop performance. The method ensures that the optimal reconstructed errors of the important feedback states are totally unaffected by the reduction of the order of the observer.

References

[1]Villemagne, C. R., and Skeleton, R. E., "Controller Reduction Using Canonical Interactions," *IEEE Transactions on Automatic Control*, Vol. 33, No. 8, 1988, pp. 740–750.

[2]Skeleton, R. E., and Yousuff, A., "Component Cost Analysis of Large Scale Systems," *International Journal of Control*, Vol. 37, No. 2, 1983, pp. 285–304.

[3]Yousuff, A., and Skeleton, R. E., "Controller Reduction by Component Cost Analysis," *IEEE Transactions on Automatic Control*, Vol. AC-29, No. 6, 1984, pp. 520–530.

[4]Nissim, E., "Order Reduction of Linear-Quadratic-Gaussian-Designed Controllers," *Journal of Guidance, Control, and Dynamics*, Vol. 16, No. 6, 1993, pp. 1154–1161.

[5]Doyle, J. C., and Stein, G., "Robustness with Observers," *IEEE Transactions on Automatic Control*, Vol. AC-24, No. 4, 1979, pp. 607–611.

[6]Hwang, C., Winter, B., and Mills, G., "Demonstration of Active Wing/Store Flutter Suppression Systems," AFFDL-TR-78-65, 1978.

[7]Roger, K. L., "Airplane Math Modelling Methods for Active Control Design," AGARD CP-228, Aug. 1977.

Approximations for Quantitative Feedback Theory Designs

D. K. Henderson* and R. A. Hess†
University of California, Davis, Davis, California 95616-5294

Introduction

QUANTITATIVE feedback theory (QFT) is a powerful technique for the design of multi-input/multi-output (MIMO) flight control systems, which guarantees performance and stability robustness in the presence of significant parametric uncertainty in the vehicle model.[1] The performance specifications can be stated in either the time or the frequency domain, with the latter being more common. In employing QFT in the frequency domain, the designer must specify bounds on the amplitude ratios of on-axis and off-axis response-to-command transfer functions (desired tracking performance and desired cross-coupling minimization). Whereas specifying tracking bounds is fairly straightforward, especially in flight control problems where handling qualities specifications can provide some guidance, the specification of cross-coupling bounds

Received Oct. 9, 1996; revision received March 20, 1997; accepted for publication April 9, 1997.

*Graduate Student, Department of Mechanical and Aeronautical Engineering; currently Senior Engineer/Scientist, McDonnell Douglas Corp., Long Beach, CA 90807. Member AIAA.

†Professor, Department of Mechanical and Aeronautical Engineering. Associate Fellow AIAA.

can be problematic. This is not a minor concern as these cross-coupling bounds can drive the entire QFT design. Finally, MIMO QFT designs are usually approached using a sequential loop closure technique to minimize conservatism.[2] Until now, no method other than trial and error could be employed to determine the loop closure sequence. As will be seen, both the problem of determining cross-coupling bounds and loop closure sequence can be solved using an approximate predesign technique (PDT).

Flight Control Example

Consider Fig. 1, which shows a feedback topology for the design of a lateral-directional flight control system for a supermaneuverable fighter. A single diagonal compensation matrix $G_{\mathrm{QFT}}(s)$ is to provide performance and stability robustness across a variety of flight conditions. Here, $P(s)$ represents a 2×5 plant matrix with outputs of sideslip β and roll rate p. There are five control effectors: differential horizontal stabilator, yaw thrust vectoring, differential pitch thrust vectoring, aileron, and rudder. The matrix S is a 5×2 control distribution matrix. Also shown is an inner, yaw-rate r feedback loop, which has been closed with a fixed compensator $G_r(s)$. The matrix $G_c(s)$ is a constant 2×2 precompensation matrix, which approximately decouples the plant across the flight conditions being studied.[3] Finally, the matrix $F(s)$ is a diagonal 2×2 prefilter matrix. The goal of the QFT design is to specify the diagonal elements of $G_{\mathrm{QFT}}(s)$ and $F(s)$ to meet performance and stability requirements in the presence of the uncertainty in $P(s)$ introduced by considering 15 different flight conditions.

PDT

Approximately Decoupled Controls

The PDT has its basis in an assumption regarding the diagonal compensation elements of $G_{\mathrm{QFT}}(s)$. Referring to the example, if the pseudocontrols u_β and u_p are approximately decoupled, then the following relationship can be employed:

$$G_{\mathrm{QFT}_{\beta\beta}} \approx \left(\omega_{c_\beta}/s\right) \cdot [1/(\beta/u_\beta)]$$
$$G_{\mathrm{QFT}_{pp}} \approx \left(\omega_{c_p}/s\right) \cdot [1/(p/u_p)] \tag{1}$$

where the double subscripts on the left-hand sides of the equations represent diagonal elements and the $\omega_{c_{(-)}}$ represent crossover frequencies. Equation (1) exploits the well-known fact that the loop transmission $L(s)$ of a well-designed single-input/single-output system, or the loop transmissions of a decoupled MIMO system, each resemble $\omega_{c_{(-)}}/s$ near the region of crossover. Equation (1) extends this approximation to all frequencies. In terms of approximating the elements of $G_{\mathrm{QFT}}(s)$, low-frequency characteristics ($\omega \ll \omega_c$) are relatively unimportant provided $|L(j\omega)| \gg 1.0$, and the high-frequency characteristics ($\omega \gg \omega_c$) are relatively unimportant provided $|L(j\omega)| \ll 1.0$. These conditions are guaranteed by Eq. (1). For QFT designs, a nominal plant is selected to define a nominal loop transmission on the Nichols chart. For the PDT, this simply means choosing one of the possible plants out of the uncertain set to define the denominator of the right-hand sides of Eq. (1).

The PDT is limited to minimum phase systems, or at least those possessing no low-frequency zeros in the right-half plane. Thus, the diagonal elements of $P \cdot S \cdot G_c(s)$ should have no right-half plane zeros at or below the loop crossover frequency.

Coupled Controls

If a precompensator $G_c(s)$ is not being employed, and if the plant itself is not adequately decoupled, the relation of Eq. (1) may have to be modified to account for the control cross coupling that may exist. In such a case, Eq. (1) becomes

$$G_{\mathrm{QFT}_{\beta\beta}} \approx \frac{\omega_{c_\beta}}{s} \cdot \frac{1}{(\beta/u_\beta)_{p \to u_p}}, \qquad G_{\mathrm{QFT}_{pp}} \approx \frac{\omega_{c_p}}{s} \cdot \frac{1}{(p/u_p)_{\beta \to u_\beta}} \tag{2}$$

The subscripts on the parenthetic terms in the denominators on the right-hand sides of Eqs. (2), e.g., $p \to u_p$, mean that, in calculating the transfer function in parentheses, the remaining control loop is closed. In the analysis, one of the compensators will have to be determined first, and the compensation in the remaining loop will be unknown. The most expedient course is simply to approximate the unknown compensator by the appropriate relation in Eq. (1).

Implementation

In employing the PDT as part of a QFT design, a relatively simple implementation procedure can be followed, here couched in terms of the flight control example of Fig. 1.

1) Tracking performance bounds are selected. Initial estimates for the crossover frequencies ω_{c_β} and ω_{c_p} are chosen. Approximations for the diagonal compensation elements in $G_{\mathrm{QFT}}(s)$ are created from either Eqs. (1) or (2). With approximations for the compensators thus obtained, closed-loop relations for the tracking and cross-coupling transfer functions can be obtained for each flight condition. If the variations in the amplitude of the tracking transfer functions across all of the flight conditions exceed the bounds at some frequency or frequencies within the range of interest, then the crossover frequencies are increased and the procedure repeated. When the variations are acceptable, elements in the prefilter matrix $F(s)$ can be determined so that the actual tracking transfer function amplitudes lie within the prescribed bounds.

2) Next is cross-coupling minimization. After completing step 1, the amplitudes of the closed-loop cross-coupling transfer functions can be obtained for each flight condition. Least-upper bounds on these amplitudes will provide realistic bounds for cross-coupling minimization for the formal QFT design. Of course, if cross-coupling bounds are available ab initio (typically an unlikely event), then crossover frequency selection in step 1 is predicated on meeting these as well as the tracking bounds.

3) Last is cost of feedback. An examination of the predicted compensation from Eqs. (1) or (2) in the region beyond crossover provides an estimate of the sensor noise propagation to the plant inputs. This noise propagation has been called cost of feedback by Horowitz.[1]

Results

The results of the implementation of the PDT just described will be 1) estimates of the loop crossover frequencies, 2) estimates of

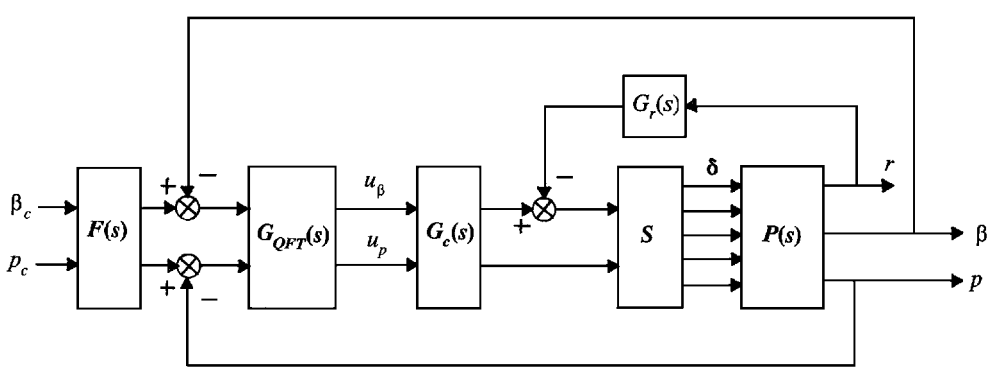

Fig. 1 MIMO lateral-directional flight control system.

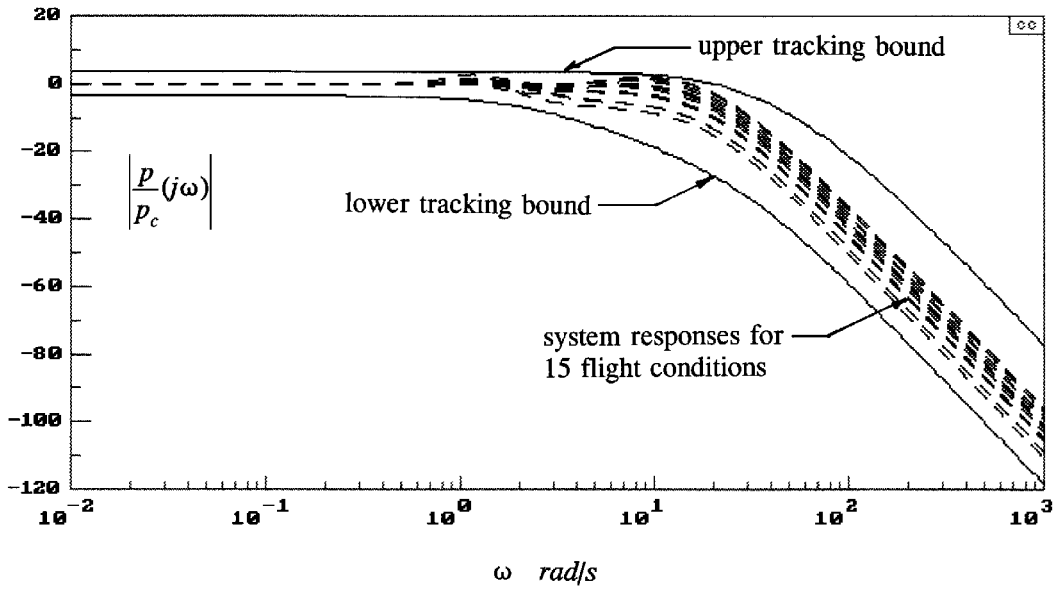

Fig. 2 Tracking performance results for roll-rate to roll-rate command with PDT for 15 flight conditions.

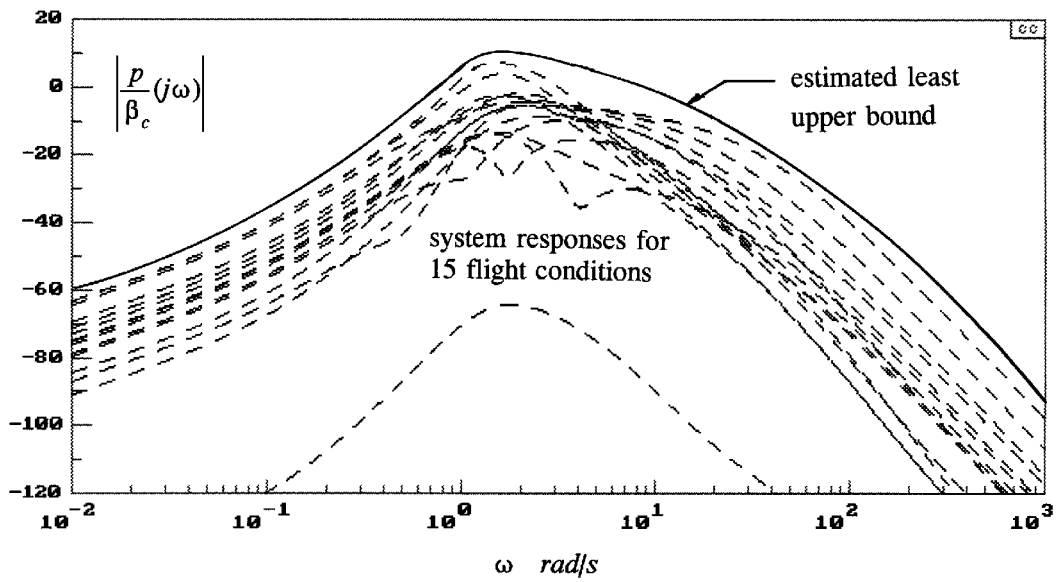

Fig. 3 Cross-coupling minimization for roll-rate to sideslip command with PDT for 15 flight conditions.

the required compensation and prefilters (with cost of feedback), 3) estimates of realistic cross-coupling bounds to be used in the formal QFT procedure, and 4) a suggested loop closure sequence for the formal QFT procedure. Because the formal QFT procedure will likely involve sequential loop closure, and because this first loop closure involves the most conservatism, the loop with the lower estimated crossover frequency should be the first to be closed in the formal QFT design.

Application to the Flight Control Example

Tracking performance bounds were selected for the flight control example outlined earlier, and the steps just outlined were performed. Figure 2 shows the estimated roll-rate tracking performance that resulted, i.e., $|(p/p_c)(j\omega)|$ for the 15 flight conditions considered. Figure 3 shows the estimated cross coupling between roll-rate and sideslip command, i.e., $|(p/\beta_c)(j\omega)|$. A suggested bound to be used in the formal QFT design is also shown. The estimated crossover frequencies that yielded the performance shown were $\omega_{c_\beta} = 3.0$ rad/s and $\omega_{c_p} = 6.0$ rad/s. These values suggest that the β loop should be closed first in the formal QFT design. An examination of the elements of the total compensation matrix $G_c \cdot G_{\mathrm{QFT}}(s)$ indicates that the β loop will involve a considerably higher cost of feedback than the p loop.

The results of predesign exercises as described have compared quite favorably with those obtained in formal QFT designs that entailed none of the approximations used in the PDT.[3]

Conclusions

The computational requirements for obtaining the results summarized in the preceding section were very modest and were easily accomplished using computer-aided control system design software. Of special significance is the ability of the PDT to indicate a loop closure sequence for MIMO QFT designs that employ sequential loop closure. Although discussed as part of a 2×2 design, the PDT is obviously applicable to designs with a greater number of inputs and system responses.

Acknowledgments

This research was supported by NASA Langley Research Center under Grant NAG1-1744. Barton Bacon was the Contract Technical Manager.

References

[1] Horowitz, I., *Quantitative Feedback Design Theory (QFT)*, QFT Publications, Boulder, CO, 1993, Chap. 14.

[2]Horowitz, I., "Improved Design Technique for Uncertain Multiple-Input, Multiple-Output Feedback Systems," *International Journal of Control*, Vol. 36, No. 6, 1982, pp. 977–988.

[3]Henderson, D. K., "Multi-Input, Multi-Output Flight Control Design Using Pseudo-Control, Software Rate Limiters, and Quantitative Feedback Theory," Ph.D. Dissertation, Dept. of Mechanical and Aeronautical Engineering, Univ. of California, Davis, CA, 1996.

Verifying Robust Time-Optimal Commands for Multimode Flexible Spacecraft

Lucy Y. Pao*
University of Colorado, Boulder, Colorado 80309
and
William E. Singhose†
Massachusetts Institute of Technology, Cambridge, Massachusetts 02139

Introduction

ROBUST and nonrobust time-optimal control of flexible spacecraft has been the subject of numerous papers in recent years.[1–7] The command profiles are obtained by using a numerical optimization to minimize the command duration while satisfying a set of constraint equations. To obtain the exact time-optimal commands, a nonlinear optimization must be performed. Because nonlinear optimizations are dependent on initial guesses and are susceptible to local minima, the solutions obtained must somehow be verified. This Note presents a numerical method for checking the validity of numerically obtained command profiles.

Robust Time-Optimal Control

The time-optimal control for rest-to-rest slewing of a linear flexible system with denominator dynamics has been shown to be a multiswitch bang-bang profile.[1,3] The control has the effect of placing a zero over each of the flexible poles of the system.[5,8] Robust time-optimal commands can be generated by placing two zeros at, or near, each pole.[4–6] Robust commands are also multiswitch bang-bang functions.

For example, consider the system shown in Fig. 1 when the total mass is 1, the input force is bounded by ± 1, the low mode is 1 Hz, and the second mode is set to 4.4 Hz. The constraint equations used to determine the robust time-optimal control can be found in many sources.[4–6] Figure 2 shows the switch times of a robust command as a function of the desired slew distance x_d. The switches are shown over the small range of $1.96 \leq x_d \leq 2.06$. The number of switches and their time locations change in a complicated manner.

The robust time-optimal switch times (including the switches at the start and end of the command) for the case of $x_d = 2.02$ are

$$t_i = [0 \quad 0.042332 \quad 0.048551 \quad 1.09422 \quad 1.27463 \quad 1.42838 \quad 1.44837 \quad 1.51773 \quad 1.58709 \quad 1.60709 \quad 1.76083 \quad 1.94125 \quad 2.98692 \quad 2.99314 \quad 3.03547] \tag{1}$$

If the initial guesses used for the nonlinear optimization are changed slightly, then the optimization finds a local minima and returns switch times of

$$t_i = [0 \quad 0.05339 \quad 0.06250 \quad 1.04164 \quad 1.04313 \quad 1.10669 \quad 1.29053 \quad 1.5209 \quad 1.75127 \quad 1.93512 \quad 1.99867 \quad 2.000162 \quad 2.97931 \quad 2.98841 \quad 3.0418] \tag{2}$$

Note that command duration (the final t_i) is slightly longer than the true time-optimal command of Eq. (1). In general, local minima can yield profiles that are considerably longer and have more or fewer switches than the true time-optimal command.

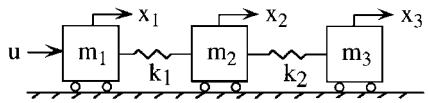

Fig. 1 Simple model of a system with two flexible modes.

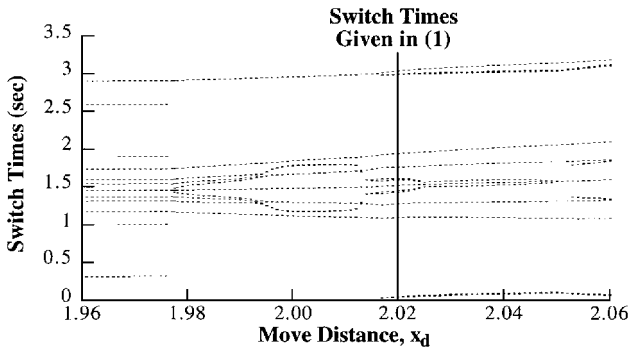

Fig. 2 Switch times as a function of move distance.

Verification of Solutions

From the preceding section, we know that the solution space for robust time-optimal control of multimode systems is very complicated. In this section, we present a method for verifying the time optimality of a prospective solution. Using this method, we can discard local minimum solutions and continue searching for the global optimal.

To verify the optimality of the nonrobust time-optimal control, we consider the system represented in the form

$$\dot{\boldsymbol{x}}(t) = \boldsymbol{F}\boldsymbol{x}(t) + \boldsymbol{g}u(t) \tag{3}$$

$$y(t) = \boldsymbol{h}\boldsymbol{x}(t) \tag{4}$$

where $\boldsymbol{F}$ is the block diagonal of $[\boldsymbol{F}_0 \ \boldsymbol{F}_1 \ \cdots \ \boldsymbol{F}_m]$, $\boldsymbol{g} = [\boldsymbol{g}_0 \ 0 \ g_1 \ \cdots \ g_m]^T$, and $\boldsymbol{h} = [\boldsymbol{h}_0 \ h_1 \ 0 \ \cdots \ h_m \ 0]$. $\boldsymbol{F}_0$, $\boldsymbol{g}_0$, and $\boldsymbol{h}_0$ represent the rigid-body dynamics and are given by

$$\boldsymbol{F}_0 = \begin{bmatrix} 0 & 1 \\ 0 & 0 \end{bmatrix} \qquad \boldsymbol{g}_0 = [0 \quad 1] \qquad \boldsymbol{h}_0 = [1 \quad 0] \tag{5}$$

$\boldsymbol{F}_1, \ldots, \boldsymbol{F}_m$ represent the m flexible modes and are given by

$$\boldsymbol{F}_j = \begin{bmatrix} 0 & 1 \\ -\omega_j^2 & -2\zeta_j\omega_j \end{bmatrix} \qquad j = 1, 2, \ldots, m \tag{6}$$

It has been shown that the double-zero robust time-optimal control is equivalent to the time-optimal control of a related flexible system that has double poles at each of the flexible poles of the original system.[5,8,9] Thus, to verify the optimality of the robust time-optimal control, we consider an augmented system where

$$\boldsymbol{F}_j = \begin{bmatrix} 0 & 1 & 0 & 1 \\ -\omega_j^2 & -2\zeta_j\omega_j & 0 & 0 \\ 0 & 0 & 0 & 1 \\ 0 & 0 & -\omega_j^2 & -2\zeta_j\omega_j \end{bmatrix} \qquad j = 1, 2, \ldots, m \tag{7}$$

$$\boldsymbol{g} = [\boldsymbol{g}_0 \quad 0 \quad g_{1a} \quad 0 \quad g_{1b} \quad \cdots \quad 0 \quad g_{ma} \quad 0 \quad g_{mb}]^T \tag{8}$$

$$\boldsymbol{h} = [\boldsymbol{h}_0 \quad h_{1a} \quad 0 \quad h_{1b} \quad 0 \quad \cdots \quad h_{ma} \quad 0 \quad h_{mb} \quad 0] \tag{9}$$

Presented as Paper 96-3845 at the AIAA Guidance, Navigation, and Control Conference, San Diego, CA, July 29–31, 1996; received Oct. 15, 1996; revision received April 18, 1997; accepted for publication April 21, 1997.

*Assistant Professor, Electrical and Computer Engineering Department. Member AIAA.

†Research Assistant, Department of Mechanical Engineering. Member AIAA.